Available online at www.sciencedirect.com
SCIENCE DIRECT®
Journal of Membrane Science 277 (2006) 186–194
journal of MEMBRANE SCIENCE
www.elsevier.com/locate/memsci

Mass transfer mechanisms and transport resistances in direct contact membrane distillation process

Surapit Srisurichan [a], Ratana Jiraratananon [a,*], A.G. Fane [b,1]

[a] *Department of chemical engineering, King Mongkut's University of Technology Thonburi, 10140 Bangkok, Thailand*
[b] *UNESCO Center for Membrane Science & Technology, The University of New South Wales, Sydney, Australia*

Received 3 March 2005; received in revised form 11 October 2005; accepted 22 October 2005
Available online 29 November 2005

Abstract

The objective of the present work was to investigate the mass transport and fouling mechanism of direct contact membrane distillation (DCMD) process. The experiments were performed on a flat sheet module using pure water and humic acid solution as feeds. The membrane employed was hydrophobic PVDF of pore size 0.22 μm.

The mass transfer models based on Dusty gas model were applied to fit the flux data and the pressure blocking filtration laws were employed to explain the membrane fouling. The results showed that molecular diffusion was the most suitable model for predicting fluxes of both laminar and turbulent flow. Fouling of the membrane by humic acid aggregates can be described by cake filtration model. The transport resistance of the feed boundary layer was higher than other resistances, and fouling resistance increased significantly with time.

Keywords: Cake filtration model; Fouling; Humic acid; Membrane distillation; Molecular diffusion

1. Introduction

Membrane distillation is a process capable of producing highly pure water. The principle of separation in membrane distillation is based on the difference in volatility of each substance, and vapor pressure difference is the driving force of the process. Direct contact membrane distillation process (DCMD) is one of membrane distillation configuration in which hydrophobic porous membrane is employed as a barrier separating heated feed and cold permeate streams. The process conditions can be controlled such that liquids cannot wet the membrane, and the vapor–liquid interface forms at the membrane pore entrance. Volatile component, usually water, vaporizes at the feed interface, diffuses through the membrane pores to the permeate interface which has lower vapor pressure, and then condenses into the permeate stream. Since the temperature of feed stream is higher than that of the permeate stream, vapor pressure difference is maintained, and the separation occurs.

In membrane distillation both heat and mass transfer from the feed side, across the boundary layer and membrane, to the permeate side. Large quantity of heat is used to vaporize the volatile component at membrane surface. It results in the difference in temperature between bulk solution and membrane surface. This phenomenon is known as temperature polarization, and may cause a significant loss in the driving force of the process. The boundary layer heat transfer coefficients can be estimated by the empirical models [1–5]. Similarly, concentration polarization or mass transfer in boundary layer is taken into account in a high concentration system. It is contributed by the accumulation of non-volatile component at membrane surface, and results in the reduction of the imposed driving force and so the mass flux. However, concentration polarization generally has only little effect on the driving force, and is always neglected [3].

There are two important mechanisms responsible for the heat transfer across the membrane, i.e. conduction through the membrane material and the vapor within the membrane pore, and transfer of the heat of vaporization associated with the vapor flux. Since there is no flux induced by the conduction of heat across the membrane, it is considered as a heat loss in the process, and should be minimized.

* Corresponding author. Tel.: +66 2 470 9221; fax: +66 2 428 3534.
E-mail address: ratana.jir@kmutt.ac.th (R. Jiraratananon).
[1] Tel.: +61 2 9385 4583; fax: +61 2 9385 5981.

0376-7388/$ – see front matter © 2005 Elsevier B.V. All rights reserved.
doi:10.1016/j.memsci.2005.10.028

Dusty gas model is generally applied to describe mass transfer across the membrane. It consists of Knudsen diffusion, molecular diffusion, surface diffusion, and viscous flow. However, surface diffusion is always neglected in membrane distillation. For DCMD, many researchers showed that molecular diffusion limited [6–9] and Knudsen-molecular diffusion transition [4,10,11] models were successfully applied to describe flux.

There are several operating parameters affecting the permeation flux in membrane distillation process [2–5,12]. The higher the feed temperature, the higher the mass flux due to the increase in vapor pressure gradient. The increase in Reynold number, induced by increasing recirculation rate, causes the decrease in temperature polarization and also concentration polarization, and consequently improves the mass flux. Flux also decreases with the increase in feed concentration because of the decrease in water activity and in heat and mass transfer coefficients in the boundary layer.

As aforementioned, most of the researches published involved transport phenomena in boundary layers and across the membrane while very little attention has been paid to fouling phenomena in MD process [13–16]. Therefore, the aims of this work are to elucidate the mechanism of mass transfer across the membrane and to study the fouling phenomena and its effect on the transport resistances in DCMD process. The linearised blocking filtration laws, which are widely used to explain the fouling mechanism in membrane processes [17,18], were chosen to applied with the membrane distillation process.

2. Theory

2.1. Heat transfer in DCMD

Heat transfer in DCMD can be considered in three steps (see Fig. 1), i.e., convective heat transfer from the heated feed solution across the boundary layer to the membrane surface ($Q = h_f(T_f - T_1)$), heat transfer across the membrane by conduction and heat assembling the vapor flow through the membrane pores ($Q = N\,\Delta H_v + k_m/\delta(T_1 - T_2)$), and convective heat transfer from the membrane surface of the permeate side across the boundary layer to the bulk of permeate solution ($Q = h_p(T_2 - T_p)$).

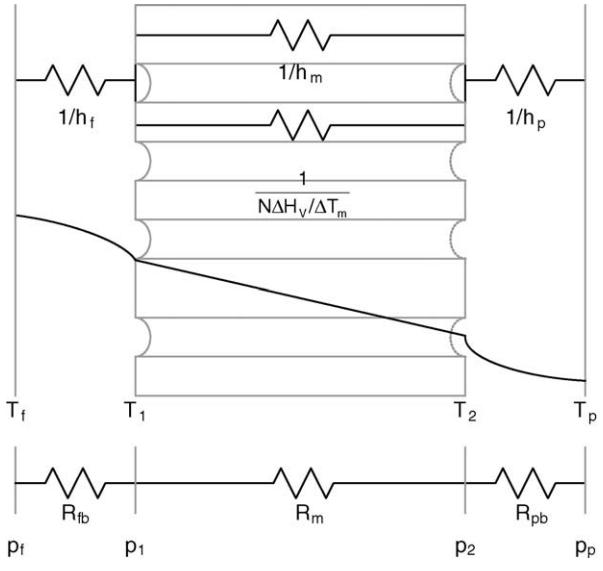

Fig. 1. Transport resistances in direct contact membrane distillation process.

From the heat balance, at steady state, T_1 and T_2 can be estimated by

$$T_1 = \frac{h_m(T_p + (h_f/h_p)T_f) + h_f T_f - N\,\Delta H_v}{h_m + h_f(1 + h_m/h_p)} \quad (1)$$

$$T_2 = \frac{h_m(T_f + (h_p/h_f)T_p) + h_p T_p + N\,\Delta H_v}{h_m + h_p(1 + h_m/h_f)} \quad (2)$$

The heat transfer coefficients in boundary layers are calculated by the empirical models. For laminar flow ($Re < 2100$) in a flat membrane module, the Graetz–Leveque is recommended [2–4]:

$$Nu = 1.86\left(Re\,Pr\frac{d_h}{L}\right)^{0.33} \quad (3)$$

In contrast, the heat transfer coefficients for the turbulent flow ($2500 < Re < 1.25 \times 10^5$, and $0.6 < Pr < 100$) are evaluated by

$$Nu = 0.023 Re^{0.8}\,Pr^n \quad (4)$$

where n is a constant, and equals to 0.4 for heating and 0.3 for cooling, respectively [19].

2.2. Mass transfer across the membrane

Mass transfer in direct contact membrane distillation (DCMD) can also be separated into three steps, e.g. mass transfer in feed boundary layer, mass transfer across the membrane, and mass transfer in permeate boundary layer. The mass transfer in permeate boundary layer is not taken into account since the mole fraction of the transporting species in the permeate stream is approximately equal to one. The mass transfer in boundary layers is analyzed by film theory while Dusty gas model (DGM) is usually employed to describe the mass transfer across the membrane. Dusty gas model elucidates mass transfer in porous media by four possible mechanisms: viscous flow, Knudsen diffusion, molecular diffusion, and surface diffusion. It is general for DCMD application to neglect surface diffusion and viscous flow [1]. The model can be further simplified in the specific cases. Knudsen diffusion model is suitable for the system that the collision between molecule and pore wall dominates the mass transport, and is given by

$$N' = \frac{1}{RT}\frac{2\,\varepsilon r}{3\tau}\left(\frac{8RT}{\pi M_i}\right)^{1/2}\frac{(p_1 - p_2)}{\delta} \quad (5)$$

On the other hand, molecular diffusion model is preferred when the collision between the molecules plays main role in the mass transfer across the membrane:

$$N' = \frac{\varepsilon}{\tau\delta}\frac{PD_{ij}}{RT}\frac{(p_1 - p_2)}{|p_a|_{ln}} \quad (6)$$

Table 1
Blocking filtration laws

Blocking filtration laws	n	Linearised equation	Assumption
Complete blocking model	2	$-\ln\left(\frac{J_0}{J}\right) - 1 = Kt$	Each particle reaching the membrane surface blocks a membrane pore
Intermediate blocking model	1	$\frac{J_0}{J} - 1 = Kt$	Each particle reaching the membrane probably blocks the pore
Standard blocking model	3/2	$\sqrt{\frac{J_0}{J}} - 1 = Kt$	Pore volume decreases due to the deposition of particles on pore walls
Cake filtration model	0	$\left(\frac{J_0}{J}\right)^2 - 1 = Kt$	The overall resistance of the process is composed of a membrane resistance, which is unchanged, and a cake resistance

Nevertheless, if both molecule-pore wall and molecular–molecular collisions occur frequently, the Knudsen-molecular diffusion transition model must be employed:

$$N' = \frac{\varepsilon PD_{ij}}{\tau\delta RT} \ln\left(\frac{p_a^2 \frac{2r}{3}\left(\frac{8RT}{\pi M_i}\right)^{1/2} + PD_{ij}}{p_a^1 \frac{2r}{3}\left(\frac{8RT}{\pi M_i}\right)^{1/2} + PD_{ij}}\right) \quad (7)$$

Both molecular diffusion limit and Knudsen-molecular diffusion transition model were successfully applied to describe the flux in DCMD system [4,6–11].

2.3. Fouling phenomena

Proposed by Hermia [20], the blocking filtration laws are widely employed for elucidating the fouling phenomena in membrane processes [17,18,21,22]. In fact, the blocking filtration laws were derived for the dead-end filtration. By adding the cake erosion model, they can also be applied to the crossflow filtration mode. The original form of the blocking filtration laws can be given as follows:

$$\frac{d^2t}{dV^2} = K\left(\frac{dt}{dV}\right)^n \quad (8)$$

where V is the volume of permeate at time t and K is the coefficient depending on the flow rate and solution properties. The parameter n is a constant depending on the fouling mechanism involved in the system, and the models are summarized in Table 1.

3. Expermiental

The experimental setup is depicted in Fig. 2. Two flat sheet membrane modules were employed. The laminar module had effective membrane area and the hydraulic diameter (d_h) of 4×10^{-3} and 4.7×10^{-3} m, respectively. The other module with hydraulic diameter of 3×10^{-3} m is referred as turbulent module. Its effective membrane area was 3.0×10^{-4} m^2. The feed was preheated in the thermostatic bath and brought to contact with the membrane by peristaltic pump. In contrast, the permeate stream was pumped through the cooling coil to adjust its temperature before passing through the permeate channel of the module. The bulk temperatures reported were the average values of the temperatures measured at the entrance and exit of each stream. The differences between inlet and outlet temperatures of both streams did not exceed 1.6 °C.

The experiments were carried out in both laminar and turbulent regions. The crossflow velocities were monitored by rotameters. The feed operating temperature ranged between 40 and 70 °C, while the temperature of permeate stream was fixed at 20 °C. The operating temperatures were controlled to be ±0.5 °C of the desired values. Pure water and humic acid solution (100 mg/l) containing natural salts (NaCl and $CaCl_2$) were feed solutions used in the experiments. Humic acid, Cat. No. H16752, was purchased from Aldrich Chemical Co. NaCl was used for adjusting the ionic strength of the humic acid solutions to be at 20 mM. The $CaCl_2$ concentration in the solutions was adjusted to be 0.775, 2.665, and 3.775 mM in order to control the formation of humic acid coagulates. The pH of the solution was 7.0. The water flux was measured by the analytical balance. Since the membrane wetting is prohibited in membrane distillation process, the conductivity of the permeate was periodically measured in order to ensure that there was no penetration of the process liquid through the membrane pores.

The membrane used in the experiments was hydrophobic PVDF membrane (GVHP, purchased from Millipore Inc.). The porosity, average pore radius, and membrane thickness provided by the supplier were 0.75, 0.11, and 125 μm, respectively. The thermal conductivity of the membrane (k_m) is 0.041 W/mK [4].

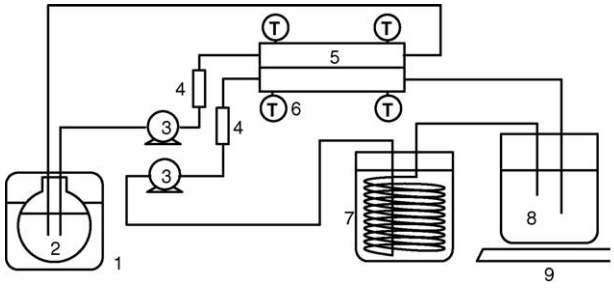

Fig. 2. Membrane distillation setup: (1) water bath; (2) feed reservoir; (3) peristaltic pumps; (4) rotameters; (5) flat-sheet module; (6) thermocouples (T); (7) cooling coil; (8) permeate reservoir; (9) analytical balance.

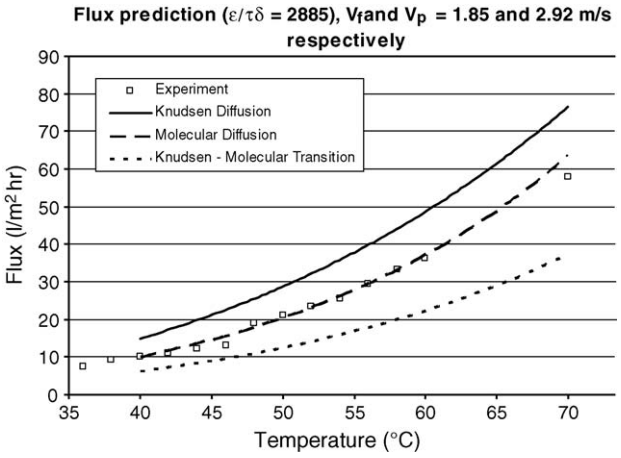

Fig. 3. Pure water flux vs. feed temperature (turbulent region).

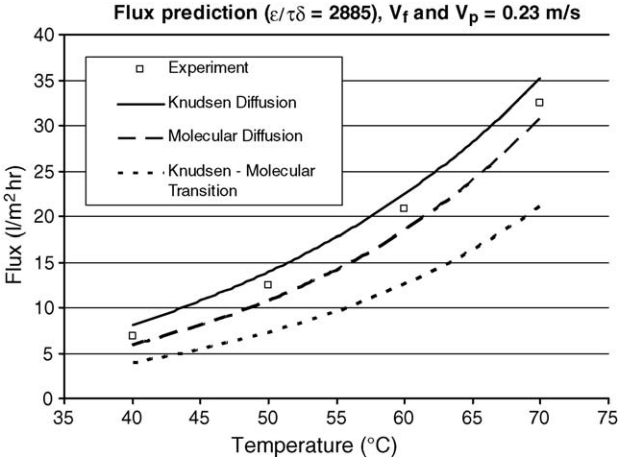

Fig. 4. Pure water flux vs. feed temperature (laminar region).

4. Results and discussion

4.1. Mass transfer and transport resistances for pure water feed

Figs. 3 and 4 depict the predicted and experimental fluxes of pure water at various feed temperatures when the system was in turbulent and laminar flow regions, respectively. For turbulent region, the experimental data corresponded very well with the flux estimated from the molecular diffusion model (Eq. (6)). Similarly, for laminar flow region, the data lied between the fluxes predicted by Knudsen diffusion limit model (Eq. (5)) and molecular diffusion limit model (Eq. (6)). However, it can be considered that the experimental data was in good agreement with the molecular diffusion limit since the estimated result was less than 10% lower.

The tortuosity factor (τ) plays very important role in determining the mass transport mechanism. The larger the value of tortuosity factor, the lower the permeation flux. By using Knudsen diffusion model, molecular diffusion model, and Knudsen-molecular diffusion model, the permeation flux predicted with various tortuosity factors are shown in Table 2. In comparison between the predicted and experimental fluxes, the data shows that Knudsen diffusion model corresponded with the experimental data when the value of tortuosity of 2.6 was employed, while the molecular diffusion model and Knudsen-molecular diffusion transition model well described the flux with the value of 2.08, and 1.1, respectively.

In this work, the tortuosity of 2.08 was employed and it was derived from the correlation proposed by Mackie and Meares [23] to be the most successfully correlation estimating the tortuosity of the membrane. It was also shown to be in reasonable agreement with many membrane manufactured by the phase inversion technique [24], i.e.,

$$\tau = \frac{(2-\varepsilon)^2}{\varepsilon} \tag{9}$$

This value of τ (2.08) was very close to the value of 2.1 obtained in the gas permeation experiment performed by Khayet et al. [25], and it was also close to the value of 2, which has been widely referred by many researchers [4,9,26]. The tortuosity factor of 2.08 was, therefore, the reliable value for the PVDF membrane used in this work. The calculated flux based on this value are shown in Figs. 3 and 4. It can be concluded that molecular diffusion was the dominant mechanism in mass transfer across the membrane in this work. The similar finding has been reported in the previous works [6–8]. It was also recently reported by Nagaraj et al. that the molecular diffusion was the mode of diffusion even the pore size of the membrane was as small as 0.2 μm [9].

Pure water flux for various conditions were evaluated by molecular diffusion limit (Eq. (6)), and is shown in Fig. 5. Each curve represents the predicted flux at indicated temperature, and the square symbols represent the experimental data at corresponding temperatures. It can be seen that the predicted values are in good agreement with the experimental data. Moreover,

Table 2
Experimental and estimated membrane distillation flux

T_f (°C)	Exprimental flux (kg/m^2 h)	Knudsen				Molecular				Transition			
		$\tau=1.1$	$\tau=1.6$	$\tau=2.08$	$\tau=2.6$	$\tau=1.1$	$\tau=1.6$	$\tau=2.08$	$\tau=2.6$	$\tau=1.1$	$\tau=1.6$	$\tau=2.08$	$\tau=2.6$
34	5.33	14.98	10.75	8.46	6.88	10.00	7.08	5.53	4.47	6.34	4.44	3.45	2.78
40	10.00	24.64	17.80	14.06	11.44	16.98	12.08	9.47	7.67	10.73	7.54	5.87	4.73
50	21.00	46.45	33.93	26.99	22.06	33.90	24.40	19.25	15.64	21.32	15.08	11.78	9.52
60	36.27	76.88	56.88	45.61	37.46	59.84	43.71	34.80	28.44	37.48	26.76	21.00	17.03
70	58.05	117.70	88.32	71.51	59.03	98.41	73.31	59.14	48.69	61.43	44.38	35.05	28.56

Note: $d_h = 3 \times 10^{-3}$ m; $T_p = 20$ °C; $V_f = 1.85$ m/s; $V_p = 2.92$ m/s.

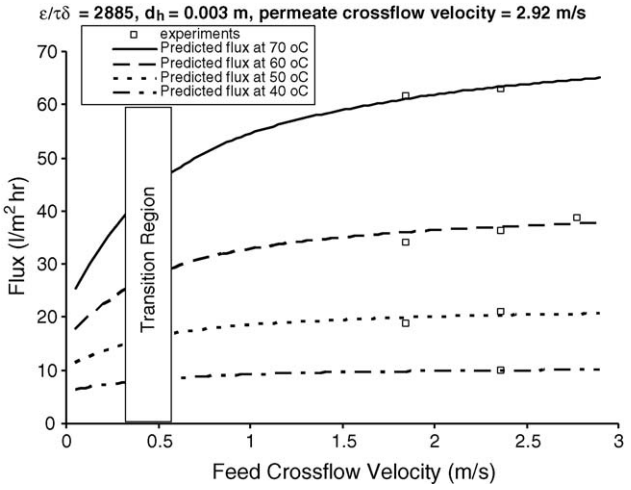

Fig. 5. Pure water flux as function of feed temperature and crossflow velocity.

Fig. 5 shows that the higher the temperature, the higher the permeation flux (see also Figs. 3 and 4). At high temperature (60–70 °C), the influence of temperature on the permeation flux was more significant compared with that of low temperature (40–50 °C) since the vapor pressure is the exponential function of the temperature.

In general, heat transfer across the feed boundary layer is often the rate limiting step for mass transfer in MD, because large quantity of heat is needed for vaporizing the liquid at the membrane surface. This leads to the temperature polarization phenomenon and the corresponding temperature polarization coefficient (TPC) is defined as:

$$\mathrm{TPC} = \frac{T_1 - T_2}{T_\mathrm{f} - T_\mathrm{p}} \tag{10}$$

The value of TPC is close to unity for well designed system that is mass transfer limited, and approaches nil for the poorly designed system that is limited by heat transfer.

Temperature polarization coefficients ranged between 0.4 and 0.53 at low crossflow velocity (0.23 m/s, laminar region) to 0.87–0.92 at high crossflow velocity (1.85 m/s, turbulent region). At high temperature, flux was much higher than at low temperature as aforementioned. Therefore, larger amount of heat was required to vaporize water at the membrane surface. This contributed to the large difference in temperature between the bulk feed stream and the membrane surface, and the pronounced effect of temperature polarization. Besides, the increase in heat transfer coefficient in boundary layer induced by the high crossflow velocity resulted in the decrease in temperature difference between bulk streams and membrane surfaces. Therefore, the permeation flux increased with the increasing crossflow velocity.

In membrane distillation process, the total resistance without the presence of fouling layer is composed of the resistance in feed boundary layer (R_fb), resistance in permeate boundary layer (R_pb), and the resistance of membrane (R_m) (see Fig. 1). Since the vapor pressure is the function of temperature, by the iteration method, the temperatures at all positions were obtained, and the resistances can be evaluated as follows:

Table 3
Resistances in membrane distillation system

T_f (°C)	V_f (m/s)	V_p (m/s)	T_1 (°C)	T_2 (°C)	R_fb	R_m	R_pb
70	1.85	2.92	66	23	70	416	9
50	1.85	2.92	48	21	48	474	11
70	0.23	0.23	57	37	434	390	118
50	0.23	0.23	43	27	352	480	121

Note: $T_\mathrm{p} = 20$ °C.

Feed boundary layer resistance:

$$R_\mathrm{fb} = \frac{p_\mathrm{f} - p_1}{N} \tag{11}$$

Membrane resistance:

$$R_\mathrm{m} = \frac{p_1 - p_2}{N} = \frac{1}{C} \tag{12}$$

Permeate boundary layer resistance:

$$R_\mathrm{pb} = \frac{p_2 - p_\mathrm{p}}{N} \tag{13}$$

The transport resistances were calculated as shown Table 3. The transport resistance in the feed boundary layer played important role at low crossflow velocity, and decreased with increasing crossflow velocity. Comparison between systems operating at different feed temperature revealed the higher the feed operating temperature, the greater the resistance in feed boundary layer. This was contributed by the temperature polarization effect at high temperature. In contrast, the mass transfer coefficient across the membrane (C) is proportional to the diffusivity, which is a function of the temperature ($\mathrm{PD_{wa}} = 4.46 \times 10^{-6} T^{2334}$). This contributed in the reduction of the resistance of the membrane with increasing operating temperature.

From the data obtained, the DCMD system operating at high crossflow velocity should be an advantage as the boundary layer resistance was minimized, and the significantly higher flux can be achieved. However, the main drawback of the high crossflow velocity system was the high pressure, which can result in the risk to the membrane wetting. Thus, in the DCMD system design, the recirculation rate should be high enough to play down the polarization effect, and low enough to maintain the vapor–liquid interface.

4.2. Fouling and transport resistances

The experimental data of humic acid solutions were employed to analyze fouling of the process. Fig. 6 shows the permeation flux versus time of 100 mg/l humic acid solution containing 3.775 mM $CaCl_2$ when ionic strength was controlled at 20 mM, and pH was controlled at 7. The operating temperatures were 70 and 20 °C for feed and permeate streams, respectively. In order to clearly see the effect of fouling on flux, the experiments were conducted in laminar region. Feed and permeate flow rates were set at 0.23 m/s. After 9 h, the permeate flux decreased from 33.6 to 22.3 l/m^2 h ($J/J_0 = 0.67$), and the membrane was covered by the dark brown layer. Since the Ca^{2+} concentration in the system was higher than critical coagulation concentration

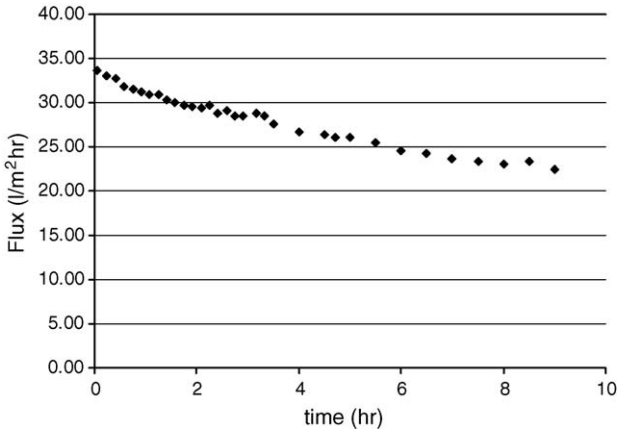

Fig. 6. Membrane distillation flux of 100 mg/l humic acid solution containing 3.775 mM $CaCl_2$ (20 mM ionic strength, pH 7, T_f 70 °C, T_p 20 °C).

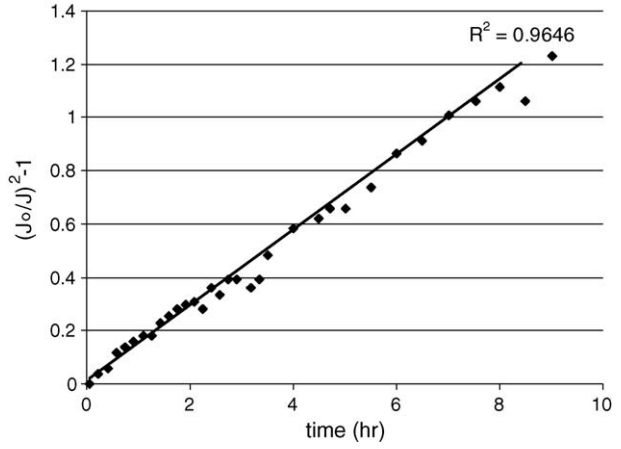

Fig. 7. Cake filtration model applying to the membrane distillation flux of 100 mg/l humic acid solution containing 3.775 mM $CaCl_2$ (20 mM ionic strength, pH 7, T_f 70 °C, T_p 20 °C).

(2–3 mM [27]), humic acid coagulates were formed and consequently resulted in deposition on the membrane surface [28–30].

Experimental data were fitted with the linearised form of blocking filtration laws aforementioned in Table 1. The experimental data agreed well with the cake filtration model for all

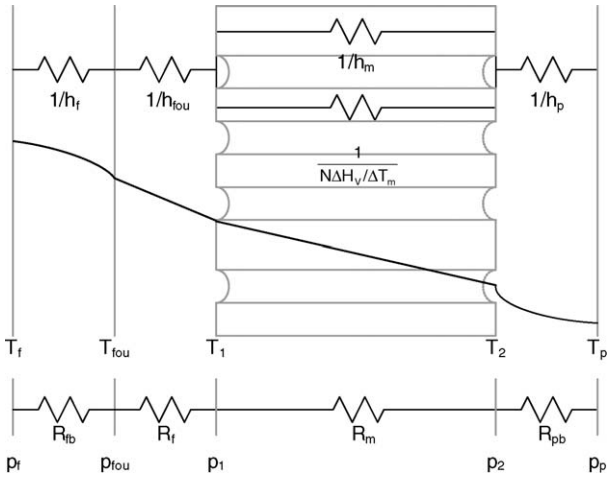

Fig. 9. Effect of fouling/cake layer on the direct contact membrane distillation system.

conditions tested as shown in Fig. 7. Since the non-wetting condition can be controlled, the humic acid coagulate deposited at the membrane surface only, but not in the pores. The accumulation of humic acid coagulate on the membrane surface formed the visible dark brown layer. The membrane was cleaned by recirculation 0.1 M NaOH through the feed channel for 2 h to recover the initial water flux. The comparison of micrographs of new and cleaned membranes taken by SEM showed that the structure of cleaned membrane was similar to that of the new membrane (see Fig. 8). Therefore, the membrane resistance was unaffected because there was no particle deposition within the pores. This corresponded with the assumption of cake filtration model, which proposes that the particles deposit onto the membrane surface in the cake form, and the change of total resistance is due to the resistance of cake layer.

With the formation of a cake layer, the conceptual diagram of the transport resistances can be shown as in Fig. 9. The time dependent fouling resistance ($R_f(t)$) can be added into the total resistance as followings:

$$R_t(t) = \frac{\Delta p_t}{N} = R_{fb} + R_f(t) + R_m + R_{pb} \quad (14)$$

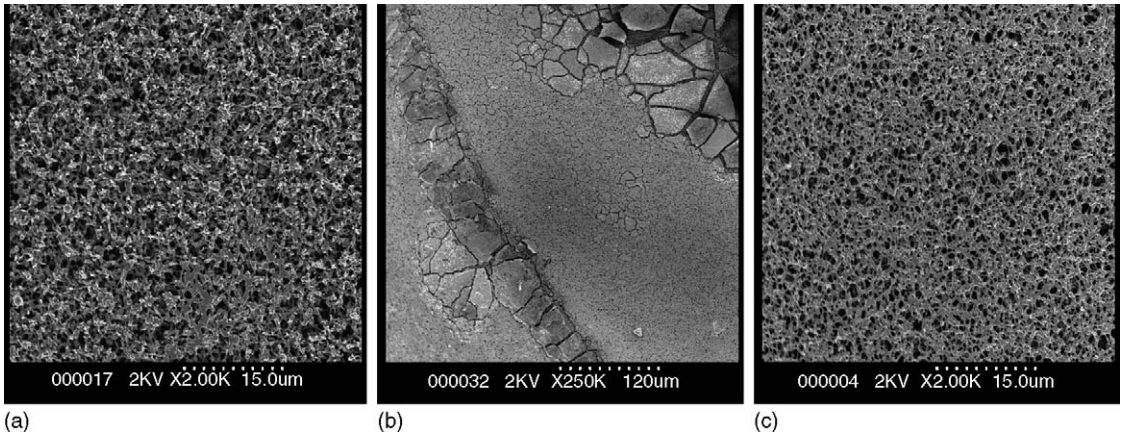

Fig. 8. Scanning electron micrographs of the membrane surfaces (2000×) of the fresh membrane (a), fouled membrane (b) and NaOH cleaned membrane (c).

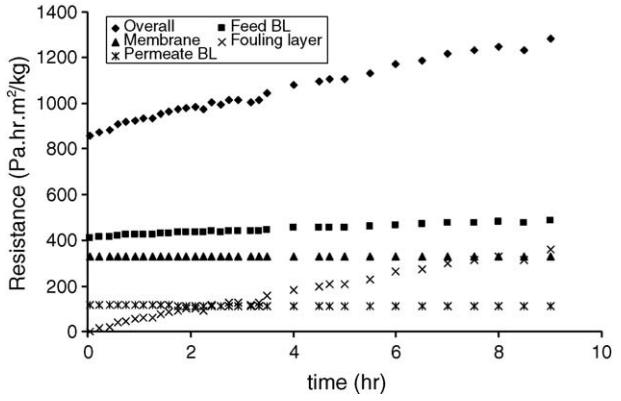

Fig. 10. Transport resistances of membrane distillation of 100 mg/l humic acid solution containing 3.775 mM $CaCl_2$ (20 mM ionic strength, pH 7, T_f 70 °C, T_p 20 °C) with respect to time.

Fig. 10 depicts the resistances of membrane distillation of 100 mg/l humic acid solution with respect to time. The result showed that the total resistance increased more rapidly at the beginning of the operation, and continued increasing with the lower rate toward the end of the experiment. The figure also shows that the resistance of the fouling layer was the cause of the increase in the total resistance of the system. The fouling resistance started from nil to 357.68 Pa m^2 h/kg, which was comparable to that of the membrane after 9 h. This revealed the significant influence of fouling/cake layer on the efficiency of membrane distillation process of humic acid solution.

The cake layer of humic acid aggregate was found to be loosely packed. It was likely that such layer did not affect mass transfer from the bulk feed stream to the membrane surface. On the other hand, the cake layer was expected to be the cause of flux decline by impeding the heat transfer in the system. The heat transfer deterioration occurs due to the additional heat transfer resistance induced by the cake layer. For example, under the conditions of T_f = 70 °C, at initial state (no fouling) T_1 and T_2 were estimated to be 56.98 and 36.92 °C. With the fouling layer (9 h), T_1 and T_2 were calculated to be 49.79 and 32.21 °C. Therefore, the difference in temperature between the bulk and feed membrane surface was increased, and TPC reduced from 0.40 (no fouling) to 0.35 (with cake layer). With the enhancement of temperature polarization, the transmembrane vapor pressure difference was reduced, and the permeation flux decreased.

From our previous study, the effect of fouling layer significantly depended on the operating conditions [28]. The concentration of Ca^{2+} presented in the solution was the most important factor. Ca^{2+} acts as a binding agent that forms complex with the humic acid molecules. This resulted in the crucial increase in size of humic acids, and consequently contributed to the more severe flux decline at high Ca^{2+} concentration due to the larger amount of deposition at membrane surface. Besides, Ca^{2+} formed coagulates when Ca^{2+} concentration exceeds the critical coagulation concentration, which was reported to be approximately 2–3 mM [27]. Table 4 presents the resistances for various conditions. It can be seen that the resistances of fouling layer increased from 0 to 22.14, 216.40, and 357.68 Pa m^2 h/kg after 9 h operation when the Ca^{2+} concentration in the solution were 0.755, 2.265, and 3.775 mM, respectively. Feed temperature was also the significant factor affecting the flux decline in membrane distillation process. The permeation flux was much higher at 70 °C than that of 50 °C, as a consequence, more amount of humic acid coagulates was retained at the membrane surface. Therefore, the fouling effect in case of high feed temperature was more significant. The resistance of fouling layer at 9 h was 92.90 and 357.68 Pa m^2 h/kg for operating at 50 and 70 °C, respectively.

Table 4
Transport resistances in membrane distillation of 100 mg/l humic acid solution, ionic strength 20 mM, at various conditions

Operating condition	Feed temperature (°C)			
	70 3.775[a]	70 2.265[a]	70 0.755[a]	50 3.775[a]
Flux				
Initial (kg/m^2 h)	33.60	30.60	31.50	10.50
9 h (kg/m^2 h)	22.50	24.00	30.60	9.45
R_t				
Initial (Pa m^2 h/kg)	858.91	943.12	916.17	953.78
9 h (Pa m^2 h/kg)	1282.64	1202.47	943.12	1059.75
$R_{at\ 9\ h}/R_{initial}$	1.49	1.28	1.029	1.11
R_{fb}				
Initial (Pa m^2 h/kg)	412.98	434.36	427.57	352.19
9 h (Pa m^2 h/kg)	485.39	480.77	432.93	364.46
R_f				
Initial (Pa m^2 h/kg)	0	0	0	0
9 h (Pa m^2 h/kg)	357.68	216.40	22.14	92.90
R_m				
Initial (Pa m^2 h/kg)	329.42	390.19	370.74	480.53
9 h (Pa m^2 h/kg)	329.42	390.19	370.74	480.53
R_{pb}				
Initial (Pa m^2 h/kg)	116.52	118.57	117.87	121.27
9 h (Pa m^2 h/kg)	110.16	115.11	117.31	121.85

Note: Laminar module, crossflow velocity = 0.23 m/s; permeate temperature = 20 °C.
[a] Ca^{2+} concentration (mM).

5. Conclusions

From the experimental data, the mechanism of water vapor transport across the membrane was shown to be molecular diffusion. Previous works also reported that molecular diffusion limit model was applied successfully to DCMD even for the membrane pore size as small as 0.2 μm [6–9].

The fouling phenomenon in membrane distillation was investigated using humic acid solution containing natural salts (NaCl and $CaCl_2$) as feed. The permeation flux measured was well fitted with the cake filtration law. This agreed with the experimental observation that cake layer was formed at the membrane surface. The cake layer resulted in the considerable increase in the resistance of the system. In case of 100 mg/l humic acid solution containing 3.775 mM $CaCl_2$, the total resistance increased from 858.91 to 1286.64 Pa m^2 h/kg after 9 h. The increase in total resistance was responsible by the presence of fouling layer resistance. For the experimental conditions studied, the percentages of R_{fb}/R_t varied from 37 to 45%, and

those of R_f/R_t ranged between 2 and 28%. Therefore, the feed boundary layer resistance controlled the permeation flux of the system.

Nomenclature

A	effective membrane area (m^2)
C	membrane distillation coefficient (kg/m^2 h Pa)
c_p	heat capacity (kJ/kg K)
D_{wa}	diffusivity of vapor in air (m^2/s)
D_{ie}^{k}	(Knudsen) diffusion coefficient (m^2/s)
D_{ije}^{o}	diffusivity (m^2/s)
d_h	hydraulic diameter (m)
ΔH_v	heat of vaporization (kJ/kg)
h_f	heat transfer coefficient in feed boundary layer (W/m^2 K)
h_m	heat transfer coefficient of membrane (W/m^2 K)
h_p	heat transfer coefficient in permeate boundary layer (W/m^2 K)
J	volumetric permeation flux (l/m^2 h)
J_0	initial volumetric permeation flux (l/m^2 h)
K	the parameter in Eq. (8)
k_m	thermal conductivity of the membrane (W/m K)
L	chamber length (m)
M_i	molecular weight (g/mol)
Nu	Nusselt number
N	permeation flux (kg/m^2 h)
N'	molar flux (mol/m^2 h)
n	parameter in Eq. (8)
Pr	Prandtl number
P	total pressure (Pa)
p_1	vapor pressure at feed membrane surface (Pa)
p_2	vapor pressure at permeate membrane surface (Pa)
p_a	partial pressure of air (Pa)
p_a^1	partial pressure of air at feed membrane surface (Pa)
p_a^2	partial pressure of air at permeate membrane surface (Pa)
p_f	vapor pressure at bluk feed (Pa)
p_{fou}	vapor pressure at the fouling surface (Pa)
p_p	vapor pressure at bluk permeate (Pa)
Q	heat flux (J/m^2 s)
R	ideal gas constant (8.314 Pa m^3/mol K)
Re	Reynolds number
R_f	resistance of fouling layer (Pa m^2 h/kg)
R_{fb}	resistance of feed boundary layer (Pa m^2 h/kg)
R_m	resistance of the membrane (Pa m^2 h/kg)
R_{pb}	resistance of permeate boundary layer (Pa m^2 h/kg)
R_t	total resistance (Pa m^2 h/kg)
r	nominal pore size (m)
T	temperature (K)
T_1	temperature at feed membrane surface (K)
T_2	temperature at permeate membrane surface (K)
T_f	temperature of bulk feed stream (K)
T_{fou}	temperature at the surface of fouling layer (K)
T_p	temperature of bulk permeate stream (K)
TPC	temperature polarization coefficient
t	time (h)
V	permeate volume (l)
v_f	crossflow velocity of feed stream (m/s)
v_p	crossflow velocity of permeate stream (m/s)

Grrek letters

δ	membrane thickness (m)
ε	porosity
μ	viscosity (Pa s)
ρ	density (kg/m^3)
τ	tortuosity

References

[1] K.W. Lawson, D.R. Lloyd, Membrane distillation, J. Membr. Sci. 124 (1997) 1–25.

[2] L. Martinez, F.J. Florido-Diaz, Theoretical and experimental studies on desalination using membrane distillation, Desalination 139 (2001) 373–379.

[3] L. Martinez-Diez, M.I. Vazquez-Gonzalez, Temperature and concentration polarization in membrane distillation of aqueous salt solutions, J. Membr. Sci. 159 (1999) 265–273.

[4] J. Phattaranawik, Heat and mass transfer models for high flux direct contact membrane distillation process, D.Eng. Thesis, Department of Chemical Engineering, King Mongkut's University of Technology Thonburi, Thailand, 2002.

[5] K.W. Lawson, D.R. Lloyd, Membrane distillation I: model design and performance evaluation using vacuum membrane distillation, J. Membr. Sci. 120 (1996) 111–121.

[6] S. Bandini, C. Gostoli, G.C. Sarti, Role of heat and mass transfer in membrane distillation process, Desalination 81 (1991) 91–106.

[7] C. Gostoli, G.C. Sarti, S. Matulli, Low temperature distillation through hydrophobic membranes, Sep. Sci. Technol. 22 (1987) 855–872.

[8] M.I. Vazquez-Gonzalez, L. Martinez, Water distillationthrough poly(tetrafluoroethylene) hydrophobic membranes in a stirred cell, J. Chem. Soc. Faraday Trans. 90 (1994) 2043–2046.

[9] N. Nagaraj, G. Patil, B.R. Babu, U.H. Hebbar, K.S.M.S. Rahavarao, S. Nene, Mass transfer in osmotic membrane distillation, J. Membr. Sci. 268 (2006) 48–56.

[10] K.W. Lawson, D.R. Lloyd, Membrane distillation II: direct contact membrane distillation, J. Membr. Sci. 120 (1996) 123–133.

[11] R.W. Schofield, A.G. Fane, C.J.D. Fell, Heat and mass transfer in membrane distillation, J. Membr. Sci. 33 (1987) 299–313.

[12] R.W. Schofield, A.G. Fane, C.J.D. Fell, R. Macoun, Factor affecting flux in membrane distillation, Desalination 77 (1990) 279–294.

[13] M. Gryta, M. Tomaszewska, J. Grzechulska, A.W. Morawski, Membrane distillation of NaCl solution containing natural organic matter, J. Membr. Sci. 181 (2001) 279–287.

[14] S.T. Hsu, K.T. Cheng, J.S. Chiou, Seawater desalination by direct contact membrane distillation, Desalination 143 (2002) 279–287.

[15] J.M. Oritz de Zarate, C. Rincon, J.I. Menugual, Concentration of bovine serum albumin aqueous solutions by membrane distillation, Sep. Sci. Technol. 33 (3) (1998) 283–296.

[16] M. Khayet, A. Velazquez, J.I. Mengual, Direct contact membrane distillation of humic acid solutions, J. Membr. Sci. 240 (2004) 123–128.

[17] P. Blanpain, M. Lalande, Investigation of fouling mechanisms governing permeate flux in the crossflow microfiltration of beer, Filtration Separation 34 (1997) 1065–1069.

[18] J. Jacob, P. Pradanos, J.I. Calvo, A. Hernandez, G. Jonsson, Fouling kinetics and associated dynamics of structural modifications, Colloids Surf. 138 (1998) 173–183.
[19] J.P. Holman, Heat Transfer, eighth ed., McGraw-Hill, Inc., 1997.
[20] J. Hermia, Constant pressure blocking filtration laws: application to power-law non-Newtonian fluids, Trans. Ind. Chem. Eng. 60 (1982) 183–187.
[21] W. Yuan, A. Kocic, A.L. Zydney, Analysis of humic acid fouling during microfiltration using a pore blockage-cake filtration model, J. Membr. Sci. 198 (2002) 51–62.
[22] R.W. Field, D. Wu, J.A. Howell, B.B. Gupta, Critical flux concept for microfiltration fouling, J. Membr. Sci. 100 (1995) 259–272.
[23] J.S. Mackie, E. Meares, Proc. R. Soc. A232 (1955) 498.
[24] S.B. Iversen, V.K. Bhatia, K. Dam-Johansen, G. Jonsson, Characterization of microporous membrane for use in membrane contactors, J. Membr. Sci. 130 (1997) 205–217.
[25] M. Khayet, K.C. Khulbe, T. Matsuura, Characterization of membrane distillation by atomic force microscopy and estimation of their water vapor transfer coefficients in vacuum membrane distillation process, J. Membr. Sci. 238 (2004) 199–211.
[26] R.W. Schofield, A.G. Fane, C.J.D. Fell, Gas and vapour transport through microporous membrane. I. Knudsen-Poiseulle transition*, J. Membr. Sci. 53 (1990) 159–171.
[27] E. Tipping, M. Ohnstad, Aggregation of aquatic humic substances, Chem. Geol. 44 (4) (1984) 349–357.
[28] S. Srisurichan, R. Jiraratananon, A.G. Fane, Humic acid fouling in the membrane distillation process, Desalination 174, 63–72, in press.
[29] W. Yuan, A.L. Zydney, Humic acid fouling during microfiltration, J. Membr. Sci. 157 (1999) 1–12.
[30] M. Kabsch-Korbutowicz, K. Majewska-Nowak, T. Winnicki, Analysis of membrane fouling in the treatment of water solutions containing humic acids and mineral salts, Desalination 126 (1999) 179–185.